


# Phase noise reduction of a 2 $\mu\text{m}$ passively mode-locked laser through hybrid III-V/silicon integration

XIANG LI,<sup>1</sup> JIA XU BRIAN SIA,<sup>2</sup>  WANJUN WANG,<sup>2</sup> ZHONGLIANG QIAO,<sup>3</sup> XIN GUO,<sup>2</sup> GEOK ING NG,<sup>2</sup> YU ZHANG,<sup>4,5</sup> ZHICHUAN NIU,<sup>4,5,8</sup> CUNZHU TONG,<sup>6</sup> HONG WANG,<sup>2,7</sup> AND CHONGYANG LIU<sup>1,9</sup>

<sup>1</sup>Temasek Laboratories, Nanyang Technological University, Singapore 637553, Singapore

<sup>2</sup>School of Electrical and Electronic Engineering, Nanyang Technological University, Singapore 639798, Singapore

<sup>3</sup>Key Laboratory of Laser Technology and Optoelectronic Functional Materials of Hainan Province, and School of Physics and Electronic Engineering, Hainan Normal University, Haikou 571158, China

<sup>4</sup>State Key Lab for Superlattices and Microstructures, Institute of Semiconductors, Chinese Academy of Sciences, Beijing 100083, China

<sup>5</sup>College of Materials Science and Opto-electronic Technology, University of Chinese Academy of Sciences, Beijing 101408, China

<sup>6</sup>State Key Lab of Luminescence and Applications, Changchun Institute of Optics, Fine Mechanics and Physics, Chinese Academy of Sciences, Changchun 130033, China

<sup>7</sup>e-mail: ewanghong@ntu.edu.sg

<sup>8</sup>e-mail: zcniu@semi.ac.cn

<sup>9</sup>e-mail: liucy@ntu.edu.sg

Received 30 November 2020; revised 10 February 2021; accepted 10 May 2021 (Doc. ID 416007); published 9 June 2021

Passively mode-locked semiconductor lasers are promising for a wide variety of chip-scale high-speed and high-capacity applications. However, the phase noise/timing jitter of such light sources are normally high, which restricts their applications. A simple and low-cost chip-scale solution to address this issue is highly desired. In this work, a two-section GaSb-based passively mode-locked laser (MLL) emitting in the 2  $\mu\text{m}$  wavelength band with a fundamental repetition frequency of  $\sim 13.35$  GHz is presented. Dramatic phase noise reduction is achieved through its hybrid integration with a silicon photonic circuit which provides chip-scale optical feedback to the MLL. Under a fixed laser bias condition, more than  $50\times$  improvement of radio frequency linewidth to sub-kilohertz level is realized by carefully adjusting the feedback strength (via a p-i-n junction-based variable optical attenuator) and optical length of the feedback loop (via integrated heater on the silicon waveguide). The phase noise reaches  $-113$  dBc/Hz at 1 MHz offset with integrated timing jitters of 274 fs (100 kHz to 100 MHz) and 123 fs (4 to 80 MHz). At the same time, the pulse-to-pulse jitter reaches as low as 7.8 fs/cycle. These values are record low for 2  $\mu\text{m}$  passively mode-locked semiconductor lasers. Our results prove the feasibility of MLL noise reduction with the chip-scale hybrid III-V/silicon integration method, bringing low-noise light sources to the silicon platform. Moreover, this work also suggests the potential miniaturization of various other functional setups with the same method. © 2021 Optical Society of America under the terms of the [OSA Open Access Publishing Agreement](#)

<https://doi.org/10.1364/OPTICA.416007>

## 1. INTRODUCTION

Passively mode-locked semiconductor lasers based on III-V materials, with their capability in generating multi-gigahertz optical pulse trains, compact footprint, flexible wavelength tuning, convenient electrical pump, etc., have become promising light sources in a wide variety of applications such as high-capacity optical communications, high-density optical storage, high-speed electro-optic sampling, optical clocking for electronic circuits, etc. [1–4]. But due to lack of external reference source, the phase noise/timing jitter of such lasers are normally high, which limits the time resolution or data transmitting capacity when they are used in the above applications. Hybrid mode locking is a way to solve this problem [5]. However, the external radio frequency (RF) sources

will increase the operation cost and in addition, applying RF signal at high frequency may become inefficient [6]. Another solution can be the use of optical injection with narrow-linewidth lasers (both single tone and dual tone) [7,8] or another mode-locked laser (MLL) [9]. But again, the use of external light sources increases the cost and complicates the setup. In contrast, self-optical injection by feeding a part of the laser emission back into the laser enables noise reduction without the use of external light sources. Its mechanism has been theoretically described with a coupled external cavity model in [10], and several results obtaining RF linewidth around 1 kHz level have been reported with this method [11–14]. However, most of these experimental studies are with fiber-/free-space-based setups. They are usually bulky and contain discrete components, which potentially limits their viability in many of

the above-mentioned applications where a chip-scale formfactor is required. To our knowledge, there is no such chip-scale self-optical feedback demonstration obtaining sub-kilohertz RF linewidth that has been reported.

In the meanwhile, silicon photonics has evolved rapidly and attracted increasing attention in the past decade and has become the most mature photonics platform due to its complementary metal-oxide-semiconductor (CMOS) compatibility. It also exhibits a large degree of design freedom, enabling the demonstration of most fundamental functional components to provide an exciting solution for chip-scale optics [15]. But as known, one intrinsic drawback of the silicon platform is its lack of light emission capability.

Based on the above, the achievement of self-optical feedback setup with the silicon photonics-based functional photonic circuits has become particularly attractive. It will dramatically reduce the setup footprint and at the same time, bring low-noise pulse trains as well as multi-wavelength light sources to the silicon platform. To do this, an effective integration method of these two material systems is highly desired. To date, there are several pathways to do III-V/silicon integration: the hybrid method with edge coupling [16–18], the heterogeneous method with wafer bonding [19–21], the epitaxial method via hetero-epitaxial growth [22,23], etc. All these pathways are with their pros and cons, and regarding the one we use in this work, the hybrid method reduces fabrication complexity, and provides thermal isolation to allow for individual optimization of III-V and silicon photonic chips. With this method, we have demonstrated external cavity tunable lasers covering a large range of wavelengths [18,24].

In this work, a two-section GaSb-based single quantum well (SQW) passively mode-locked laser is presented. The laser emission is in the 2  $\mu\text{m}$  wavelength band which is attracting significant attention due to its potential in medicine, gas sensing, free-space optical communications, hollow-core fiber-based advanced telecommunications, eye-safe light detection, and ranging (LIDAR), etc. [25–27]. For the first time, a silicon photonic circuit-based feedback loop is designed and integrated with this MLL in a hybrid formfactor to improve its phase noise. Two important parameters of this configuration, feedback strength and optical length of the feedback loop, are systematically investigated and the experimental results are discussed.

## 2. FREE-RUNNING MODE-LOCKED LASER OVERVIEW

The laser wafer used here was grown on a (100) n-GaSb substrate by molecular beam epitaxy. It comprises a 10 nm  $\text{In}_{0.2}\text{Ga}_{0.8}\text{Sb}$  SQW with 1.26% compressive strain. The detailed epitaxial structures and two-section device fabrication process are the same as described in our previous work [28]. For the device tested in this work, it has a 2.63 mm long gain section, a 0.30 mm long saturable absorber, and a 10  $\mu\text{m}$  electrical isolation area providing a  $\sim 1.1$  k $\Omega$  resistance between the two sections. Its ridge width is 5  $\mu\text{m}$ , which proves single lateral mode operation. The two facets of the MLL are as-cleaved with no coating. To achieve stable mode locking operation, the gain section and saturable absorber section need to be biased separately with a forward current ( $I_g$ ) and a reverse voltage ( $V_a$ ). During the measurements, the MLL was placed on a stage equipped with a thermoelectric cooler whose temperature was set at 20°C. To characterize the MLL, its output light from the

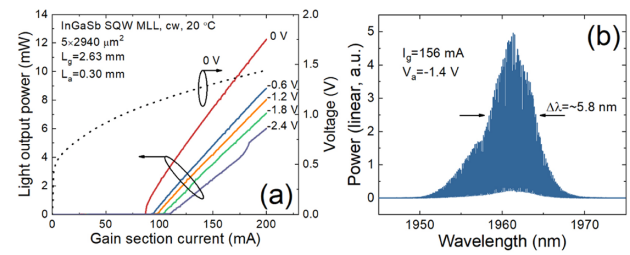


**Fig. 1.** (a) L-I curves of the free-running tested laser (one facet) when  $V_a$  was varied from 0 (unconnected) to  $-2.4$  V. The I-V curve at  $V_a = 0$  V is also shown in the figure. (b) One example of the optical spectrum when the laser works in the stable mode locking regime ( $I_g = 156$  mA,  $V_a = -1.4$  V).

absorber section facet was coupled into a single-mode fiber. The RF spectra and phase noise spectra were measured using a high-speed photodetector (EOT, ET-5000F) followed by a 50 GHz electrical spectrum analyzer (Agilent, N9030A), while the optical spectra were recorded by an optical spectrum analyzer (Yokogawa, AQ6375).

Stable mode locking was achieved in the free-running tested laser under a variety of bias conditions. Figure 1(a) shows the light output power-current (L-I) curves of the laser (one facet) in the continuous wave mode when  $V_a$  was varied from 0 (unconnected) to  $-2.4$  V. The consistent threshold current increase with increasing negative  $V_a$  is owing to the higher loss introduced by the absorber. When the absorber is unconnected, the L-I curve exhibits a turn-on jump at lasing threshold, which is widely observed in devices with a saturable absorber [29–31]. This jump is attributed to the rapid increase of photon density as the lasing action starts, which decreases the absorption of the saturable absorber since the electric field is not strong enough to sweep the carriers out of the quantum well region immediately. The current-voltage (I-V) curve under this condition is also shown in the figure. One example of the optical spectrum when the laser works in stable mode locking regime ( $I_g = 156$  mA,  $V_a = -1.4$  V) is shown in Fig. 1(b). The spectrum centering at  $\sim 1961$  nm has a full width at half-maximum of  $\sim 5.8$  nm, which indicates at least 34 longitudinal modes are locked in phase considering a longitudinal mode spacing of  $\sim 0.17$  nm.

## 3. SILICON PHOTONIC CIRCUIT-BASED FEEDBACK SETUP

The schematic of the silicon photonic circuit-based feedback setup is shown in Fig. 2(a). The silicon photonic chip is fabricated from a standard silicon-on-insulator wafer with a 220 nm thick silicon device layer via a CMOS process line. Light emitted from the gain section facet was coupled into the silicon photonic circuit. For the main part of the circuit, a rib waveguide with 600 nm width and 135 nm etch depth was used, while to facilitate the coupling by mode matching, a thin slab waveguide ( $6 \times 0.085 \mu\text{m}^2$ ) was used at the coupling port followed by a taper structure-based spot size converter (SSC) to convert the slab to the rib waveguide mode. The length and tip width of the taper structure were optimized to be 200 and 0.15  $\mu\text{m}$ , respectively.  $\sim 80\%$  of the coupled light power enters the main feedback loop while the rest  $\sim 20\%$  was tapped out into a monitoring port. This port is used to guide the alignment between the MLL and the silicon photonic chip as well as to make sure that this alignment maintains well during the testing. With

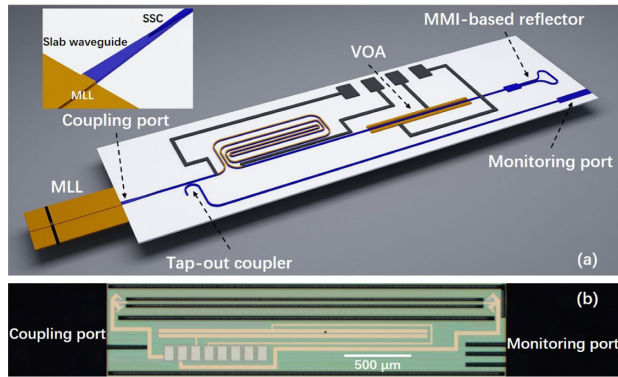


**Fig. 2.** (a) Schematic of the silicon photonic circuit-based feedback setup. (b) Microscope image of the silicon photonic circuit.

regards to the main feedback loop, a 120 nm thick TiN heater was mounted on top of it (separated from the waveguide by 1.2 μm thick SiO<sub>2</sub> cladding) to fine tune the effective refractive index of the silicon waveguide and thus to tune its optical length. The loop also includes a p-i-n junction-based variable optical attenuator (VOA) which is a critical component used to control the feedback strength, and after which, a multi-mode interference (MMI)-based full reflector. The MMI width, length, gap between output tapers, taper length, and taper width are designed to be 6, 24.3, 3, 40, and 1.35 μm, respectively. Figure 2(b) also gives a microscope image of the fabricated silicon photonic chip.

#### 4. NOISE REDUCTION RESULTS AND DISCUSSION

With this configuration, the phase noise properties of the MLL were dramatically improved. The optimal bias condition in terms of obtaining the narrowest RF linewidth is  $I_g = 156$  mA,  $V_a = -1.4$  V,  $V_{VOA} = 1.24$  V,  $V_{heater} = 5$  V. Here  $V_{VOA}$  and  $V_{heater}$  are voltages applied to the VOA and the integrated heater, respectively. The specific explanation of them will be covered in the following paragraphs. Under this bias condition, the full range (0 to 50 GHz) RF spectrum is shown in Fig. 3(a). The fundamental repetition rate is featured by a strong RF peak with ~55 dB signal-to-noise ratio at ~13.35 GHz, corresponding to the photon round-trip time (~74.90 ps) in the 2.94 mm long laser cavity. From the detailed view of the peak together with its Lorentz fit in Fig. 3(b), an RF linewidth at least as low as ~900 Hz was achieved (RBW = 1 kHz). Figure 3(c) also gives the corresponding single-sideband (SSB) phase noise spectrum (red solid line). The phase noise reaches -113 dBc/Hz at 1 MHz offset and hits the thermal noise floor quickly after that. The integrated timing jitter was calculated with the popular von der Linde method [32], resulting in 274 fs with an integration range from 100 kHz to 100 MHz, and 123 fs with the ITU-T specified range from 4 to 80 MHz. At the same time, the pulse-to-pulse jitter was determined to be as low as 7.8 fs/cycle [33]. These values are record low for 2 μm passively mode-locked semiconductor lasers whose previous narrowest RF linewidths are at the 10 kHz level [34–36], and among the lowest for any laser of this type.

For comparison, we kept the laser bias condition unchanged and removed the silicon photonic chip to bring the MLL to the free-running case. The RF linewidth rose dramatically by over 50 times to ~48.9 kHz and the corresponding phase noise spectrum is also shown in Fig. 3(c) (blue solid line). Of course, it is

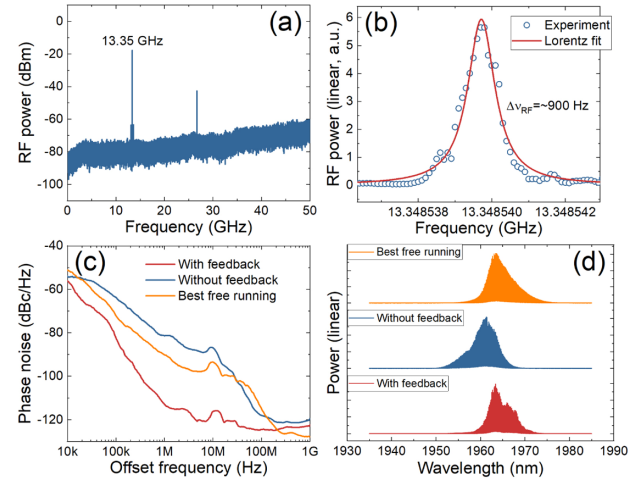


**Fig. 3.** (a) Full range (0 to 50 GHz) RF spectrum when the narrowest RF linewidth is achieved ( $I_g = 156$  mA,  $V_a = -1.4$  V,  $V_{VOA} = 1.24$  V,  $V_{heater} = 5$  V). (b) Detailed view of the RF peak at the fundamental repetition rate together with its Lorentz fit. (c) Corresponding SSB phase noise spectrum (red solid line). The phase noise spectra under the same laser bias condition when the silicon photonic chip was removed (blue solid line), and under the optimal laser bias condition in the free-running case (yellow solid line) are also shown. (d) Optical spectra corresponding to the three conditions in (c).

not necessary for the free-running laser to achieve the narrowest RF linewidth under this bias condition. This was achieved at  $I_g = 235$  mA,  $V_a = -2.33$  V with a RF linewidth of ~9.1 kHz, and the corresponding phase noise spectrum is also shown in Fig. 3(c) (yellow solid line). Optical spectra corresponding to these three conditions in Fig. 3(c) are shown in Fig. 3(d). From the figure, the lasing spectrum with feedback shows no qualitative difference from those without feedback.

Next, we will focus on one of the most critical parameters in this feedback configuration, the feedback strength (FS). Here FS is defined as the optical power injected back into the MLL from the silicon feedback loop with respect to the power emitted from one facet of the MLL. Tuning of the FS is mainly realized by applying forward-bias voltages ( $V_{VOA}$ ) to the VOA via free carrier absorption. In addition to the attenuation caused by the VOA (note that light in the feedback loop will pass the VOA twice), other attenuations of the silicon feedback loop include MLL/silicon photonic chip coupling loss at the coupling port (2.40 dB × 2), loss at the tap-out coupler (both the insertion loss of the coupler and 20% tapped out power, 1.43 dB × 2), silicon rib waveguide propagation loss (1.32 dB/cm × 5.8 cm), and loss of the full reflector (1.08 dB). All these factors result in the final feedback strength.

Figure 4(a) shows a typical evolution of the RF spectrum as a function of  $V_{VOA}$  ( $I_g = 160$  mA,  $V_a = -1.84$  V,  $V_{heater} = 5$  V). When  $V_{VOA} = 0.6$  V, which is below the turn-on voltage, no attenuation is introduced by the VOA, as shown in Fig. 4(b) in which the p-i-n junction forward current as well as attenuation (single pass) are plotted against  $V_{VOA}$ . At this time, the feedback strength equals ~ -16 dB [shown in Fig. 4(c)], resulting in a very large RF linewidth significantly greater than 100 kHz, which is even much larger than that in the free-running case. The mode locking operation is disrupted with such a strong FS. Then at  $V_{VOA} = 0.8$  V, slightly beyond the turn-on voltage, the VOA starts to introduce attenuation, as shown in Fig. 4(b). However, this attenuation is very small which just slightly improves the RF



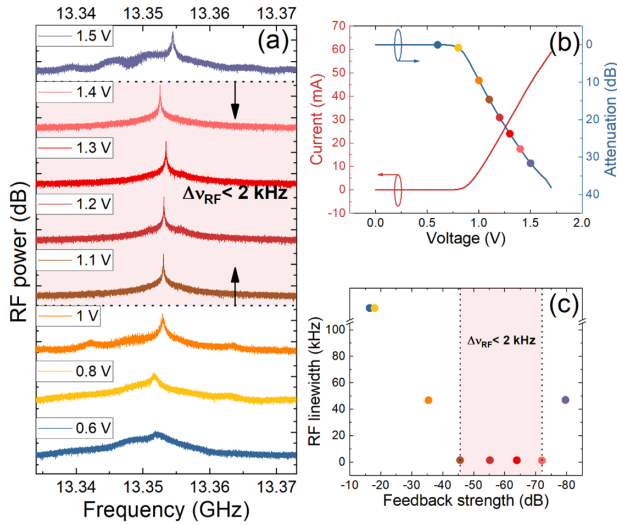


**Fig. 4.** (a) Typical evolution of the RF spectrum with  $V_{VOA}$  ( $I_g = 160$  mA,  $V_a = -1.84$  V,  $V_{heater} = 5$  V). (b) Forward current as well as introduced attenuation of the VOA (single pass) as functions of  $V_{VOA}$ . (c) RF linewidths of the RF spectra in (a) versus corresponding feedback strength.

linewidth from before. When  $V_{VOA}$  is increased to 1 V, attenuation significantly increases to result in a RF linewidth comparable to that in the free-running case. After that, as  $V_{VOA}$  is further increased to 1.1 V, the RF signal becomes very narrow and strong with a linewidth of  $\sim 1.4$  kHz. At this time, the FS is calculated to be  $\sim -46$  dB, which is within the ideal FS range in the fiber-based feedback setups [11,13]. Surprisingly, this status delivering a RF linewidth of less than 2 kHz maintains for a large range of  $V_{VOA}$  until 1.4 V when a FS of less than  $-70$  dB is determined. This FS is lower than those in the fiber-/free-space-based feedback setups (e.g.,  $> -57$  dB [13] and  $> -46$  dB [11]). We consider the reason is due to the SSC and slab waveguide which provide good mode matching to increase the feedback efficiency. After that,  $V_{VOA}$  is further increased to 1.5 V. The RF linewidth returns to the free-running level. This is reasonable as in this case the FS is so weak, just like no feedback is present.

Another important design parameter in the feedback configuration is the optical length of the feedback loop. Several works have demonstrated that in order to achieve resonant feedback to improve the phase noise properties of a MLL, the photon propagation time in the feedback loop should be an integer multiple ( $m$ ) of the round-trip time in the mode-locked laser cavity [10,37].

In the fiber-/free-space-based feedback setups, the absolute optical length of the feedback loop is unable to be precisely controlled to strictly satisfy the resonant feedback condition, but it can be changed across an entire laser cavity round-trip time (normally several tens of picoseconds) using a fiber-based tunable delay line, which will ensure the resonant feedback condition. In our silicon photonic circuit-based setup, an integrated heater is used to tune the effective index of the silicon waveguide, so optical length change across an entire laser cavity round-trip time is difficult due to limited heater power. Nevertheless, thanks to the mature silicon process, the length as well as dimensions of the silicon waveguide can be much more precisely defined by lithography. Thus, it is easy to make  $m$  closely around an integer in the original design. In our design, the physical length of the feedback loop is  $\sim 5.8$  cm, which results in an  $m$  fairly close to 6 considering an effective index

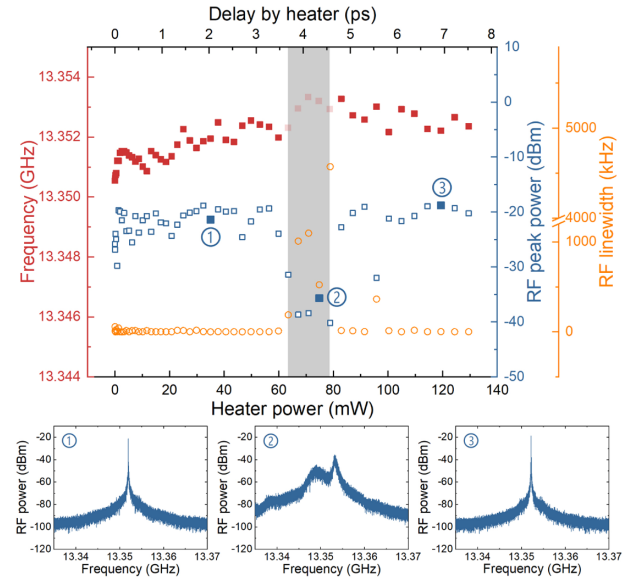


**Fig. 5.** Position of the RF signal, RF peak power, and RF linewidth as functions of the heater power ( $I_g = 160$  mA,  $V_a = -1.84$  V,  $V_{VOA} = 1.3$  V). The top x axis shows the corresponding delay. Three representative RF spectra at different heater powers are also given in the figure.

of 2.32 of the silicon rib waveguide according to simulation. The integrated heater has a heating coefficient of  $\sim 0.0003$  /mW [38], resulting in that a tuning range of  $\sim 0.039$  in the effective index can be easily achieved with a heater power of  $\sim 130$  mW ( $V_{heater} = 10$  V). This is enough to compensate any process deviations to ensure the strict satisfaction of the resonant feedback condition. This effective index tuning corresponds to a delay of  $\sim 7.54$  ps, which is  $\sim 1/10$  of the laser cavity round-trip time.

Figure 5 shows the position of the RF signal, RF peak power, and RF linewidth as functions of the heater power. The laser bias condition is  $I_g = 160$  mA,  $V_a = -1.84$  V, while the  $V_{VOA}$  is fixed at 1.3 V. Throughout this heater power range, there is no clear linear repetition frequency pulling by the delay as reported in the fiber-based setups [11,39]. The reason is  $m$  is normally larger than 1000 in the fiber-based setups, so any change caused by the tunable delay line will be diluted by 1000 times. As a result, a slight pulling of the repetition frequency (normally just a few megahertz even with the change of an entire laser cavity round-trip time) may lead to the strict satisfaction of the resonant feedback condition. In contrast, as  $m$  is only 6 in our silicon photonic circuit-based setup, even though the traveling time is only changed by  $\sim 1/10$  of the laser cavity round-trip time, this corresponds to more than 200 MHz change in the repetition frequency, which is not going to happen with this type of feedback. It is worth mentioning that according to previous experimental and numerical studies [13,37], noise reduction by self-optical feedback actually does not prefer the intrinsic exact resonant feedback condition (“intrinsic” here means “without frequency pulling”), but a range around it. At the exact resonance condition, instead of noise reduction, there may even be a rapid increase in noise. Our results in Fig. 5 also confirm this point: noise reduction is observed in most part across the heater power range indicated by strong RF peak powers around  $-20$  dBm and narrow RF linewidth except a small segment with shading. This segment should just correspond to the intrinsic exact resonant feedback condition. The corresponding variation range

of  $m$ ,  $\sim 1/10$ , is also similar to the values reported in the numerical studies, in which low-noise operation is achieved with  $m$  ranging from 6.95 to 7.05 [10] and 2.94 to 3.06 [37], respectively. This also indicates a high design/fabrication tolerance of the silicon feedback loop. Figure 5 also gives three representative RF spectra at different heater powers.

## 5. CONCLUSION

In conclusion, dramatic noise reduction of a 2  $\mu\text{m}$  GaSb-based passively mode-locked laser is achieved by chip-scale self-optical feedback based on a silicon photonic circuit. With this setup, more than  $50\times$  improvement of RF linewidth to  $\sim 900$  Hz is realized compared to the free-running case under the same laser bias condition. The phase noise ( $-113$  dBc/Hz at 1 MHz offset), integrated timing jitters (274 fs, 100 kHz to 100 MHz, and 123 fs, 4 to 80 MHz), and pulse-to-pulse jitter (7.8 fs/cycle) are record low for 2  $\mu\text{m}$  passively mode-locked semiconductor lasers. The feedback strength can be precisely controlled in a large range by the integrated p-i-n junction-based VOA. Noise reduction is achieved at relatively weak feedback strength, which may attribute to good mode matching provided by the SSC at the coupling port. The feedback loop can be very precisely defined by lithography and tuned by the integrated heater to meet the resonant feedback condition. This work proves the feasibility of MLL noise reduction with the chip-scale hybrid III-V/silicon integration method, bringing low-noise pulse trains as well as multi-wavelength light sources to the silicon platform. Moreover, with its feasibility proved, significant miniaturization of various functional setups may become possible with this edge-coupled integration method.

**Funding.** National Research Foundation Singapore (NRF-CRP12-2013-04); National Natural Science Foundation of China (61790583, 61964007); Key-Area Research and Development Program of Guangdong Province (2020B0303020001).

**Disclosures.** The authors declare that there are no conflicts of interest related to this paper.

**Data Availability.** Data underlying the results presented in this paper are not publicly available at this time but may be obtained from the authors upon reasonable request.

## REFERENCES

1. E. A. Avrutin, J. H. Marsh, and E. L. Portnoi, "Monolithic and multi-gigahertz mode locked semiconductor lasers: constructions, experiments, models, and applications," *IEE Proc. Optoelectron.* **147**, 251–278 (2000).
2. E. U. Rafailov, M. A. Cataluna, and W. Sibbett, "Mode-locked quantum-dot lasers," *Nat. Photonics* **1**, 395–401 (2007).
3. J. N. Kemal, P. Marin-Palomo, V. Panapakkam, P. Trocha, S. Wolf, K. Merghem, F. Lelarge, A. Ramdane, S. Randel, W. Freude, and C. Koos, "Coherent WDM transmission using quantum-dash mode-locked laser diodes as multi-wavelength source and local oscillator," *Opt. Express* **27**, 31164–31175 (2019).
4. K. Holc, T. Weig, W. Pletschen, K. Köhler, J. Wagner, and U. T. Schwarz, "Picosecond pulse generation in monolithic GaN-based multi-section laser diodes," *Proc. SPIE* **8625**, 862515 (2013).
5. M. Kuntz, G. Fiol, M. Laemmlin, C. Meuer, and D. Bimberg, "High-speed mode-locked quantum-dot lasers and optical amplifiers," *Proc. IEEE* **95**, 1767–1778 (2007).
6. D. Arsenijević, M. Kleinert, and D. Bimberg, "Breakthroughs in photonics 2013: passive mode-locking of quantum-dot lasers," *IEEE Photonics J.* **6**, 1–6 (2014).
7. E. Sooudi, G. Huyet, J. G. McInerney, F. Lelarge, K. Merghem, R. Rosales, A. Martinez, A. Ramdane, and S. P. Hegarty, "Injection-locking properties of InAs/InP-based mode-locked quantum-dash lasers at 21 GHz," *IEEE Photonics Technol. Lett.* **23**, 1544–1546 (2011).
8. T. Habruseva, D. Arsenijević, M. Kleinert, D. Bimberg, G. Huyet, and S. P. Hegarty, "Optimum phase noise reduction and repetition rate tuning in quantum-dot mode-locked lasers," *Appl. Phys. Lett.* **104**, 021112 (2014).
9. E. Sarailou and P. Delfyett, "Injection-locked semiconductor laser-based frequency comb for modulation applications in RF analog photonics," *Opt. Lett.* **41**, 2990–2993 (2016).
10. C. Otto, K. Ludge, A. G. Vladimirov, M. Wolfrum, and E. Scholl, "Delay-induced dynamics and jitter reduction of passively mode-locked semiconductor lasers subject to optical feedback," *New J. Phys.* **14**, 113033 (2012).
11. D. Arsenijević, M. Kleinert, and D. Bimberg, "Phase noise and jitter reduction by optical feedback on passively mode-locked quantum dot lasers," *Appl. Phys. Lett.* **103**, 231101 (2013).
12. K. Merghem, R. Rosales, S. Azouigui, A. Akrou, A. Martinez, F. Lelarge, G.-H. Duan, G. Aubin, and A. Ramdane, "Low noise performance of passively mode locked quantum-dash-based lasers under external optical feedback," *Appl. Phys. Lett.* **95**, 131111 (2009).
13. C. Lin, F. Grillot, N. A. Naderi, Y. Li, and L. F. Lester, "RF linewidth reduction in a quantum dot passively mode locked laser subject to external optical feedback," *Appl. Phys. Lett.* **96**, 051118 (2010).
14. Z. G. Lu, J. R. Liu, P. J. Poole, C. Y. Song, and S. D. Chang, "Ultra-narrow linewidth quantum dot coherent comb lasers with self-injection feedback locking," *Opt. Express* **26**, 11909–11914 (2018).
15. D. Thomson, A. Zilkie, J. E. Bowers, T. Komljenovic, G. T. Reed, L. Vivien, D. Marris-Morini, E. Cassan, L. Viot, J.-M. Fédéli, J.-M. Hartmann, J. H. Schmid, D.-X. Xu, F. Boeuf, P. O'Brien, G. Z. Mashanovich, and M. Nedeljkovic, "Roadmap on silicon photonics," *J. Opt.* **18**, 073003 (2016).
16. T. Kita, R. Tang, and H. Yamada, "Narrow spectral linewidth silicon photonic wavelength tunable laser diode for digital coherent communication system," *IEEE J. Sel. Top. Quantum Electron.* **22**, 23–34 (2016).
17. R. Wang, A. Malik, I. Šimonyte, A. Vizbaras, K. Vizbaras, and G. Roelkens, "Compact GaSb/silicon-on-insulator  $2.0\times$   $\mu\text{m}$  widely tunable external cavity lasers," *Opt. Express* **24**, 28977–28986 (2016).
18. J. X. B. Sia, X. Li, W. Wang, Z. Qiao, X. Guo, J. Zhou, C. G. Littlejohns, C. Liu, G. T. Reed, and H. Wang, "Sub-kHz linewidth, hybrid III-V/silicon wavelength-tunable laser diode operating at the application-rich 1647–1690 nm," *Opt. Express* **28**, 5134–5224 (2020).
19. G. Roelkens, L. Liu, D. Liang, R. Jones, A. Fang, B. Koch, and J. Bowers, "III-V/silicon photonics for on-chip and intra-chip optical interconnects," *Laser Photonics Rev.* **4**, 751–779 (2010).
20. T. Komljenovic, M. Davenport, J. Hulme, A. Liu, C. Santis, A. Spott, S. Srinivasan, E. Stanton, C. Zhang, and J. Bowers, "Heterogeneous silicon photonic integrated circuits," *J. Lightwave Technol.* **34**, 20–35 (2016).
21. M. L. Davenport, S. Liu, and J. E. Bowers, "Integrated heterogeneous silicon/III-V mode-locked lasers," *Photonics Res.* **6**, 468–478 (2018).
22. A. Y. Liu, J. Peters, X. Huang, D. Jung, J. Norman, M. L. Lee, A. C. Gossard, and J. E. Bowers, "Electrically pumped continuous-wave 1.3  $\mu\text{m}$  quantum-dot lasers epitaxially grown on on-axis (001) GaP/Si," *Opt. Lett.* **42**, 338–341 (2017).
23. S. Chen, M. Liao, M. Tang, J. Wu, M. Martin, T. Baron, A. Seeds, and H. Liu, "Electrically pumped continuous-wave 1.3  $\mu\text{m}$  InAs/GaAs quantum dot lasers monolithically grown on on-axis Si (001) substrates," *Opt. Express* **25**, 4632–4639 (2017).
24. J. X. B. Sia, W. Wang, Z. Qiao, X. Li, X. Guo, J. Zhou, C. G. Littlejohns, Z. Zhang, C. Liu, G. T. Reed, and H. Wang, "Compact silicon photonic hybrid ring external cavity (SHREC)/InGaSb-AlGaAsSb wavelength-tunable laser diode operating from 1881–1947 nm," *Opt. Express* **28**, 5134–5146 (2020).
25. K. Scholle, S. Lamrini, P. Koopmann, and P. Fuhrberg, *Frontiers in Guided Wave Optics and Optoelectronics*, B. Pal, (InTech, 2010), Chap. 21.
26. J. Geng and S. Jiang, "Fiber lasers: the 2  $\mu\text{m}$  market heats up," *Opt. Photonics News* **25**(7), 34–41 (2014).
27. M. N. Petrovich, F. Poletti, J. P. Wooler, A. M. Heidt, N. K. Baddela, Z. Li, D. R. Gray, R. Slavík, F. Parmigiani, N. V. Wheeler, J. R. Hayes, E. Numkam, L. Gruner-Nielsen, B. Pálsdóttir, R. Phelan, B. Kelly, J. O'Carroll, M. Becker, N. MacSuihbne, J. Zhao, F. C. G. Gunning, A. D. Ellis, P. Petropoulos, S. U. Alam, and D. J. Richardson, "Demonstration of amplified data transmission at 2  $\mu\text{m}$  in a low-loss wide bandwidth

- hollow core photonic bandgap fiber," *Opt. Express* **21**, 28559–28569 (2013).
28. X. Li, H. Wang, Z. Qiao, X. Guo, W. Wang, J. X. B. Sia, G. I. Ng, Y. Zhang, Z. Niu, C. Tong, and C. Liu, "High temperature characteristics of a 2  $\mu\text{m}$  InGaSb/AlGaAsSb passively mode-locked quantum well laser," *Appl. Phys. Lett.* **114**, 221104 (2019).
  29. X. Huang, A. Stintz, H. Li, A. Rice, G. Liu, L. Lester, J. Cheng, and M. J. Malloy, "Bistable operation of a two-section 1.3  $\mu\text{m}$  InAs quantum dot laser-Absorption saturation and the quantum confined Stark effect," *IEEE J. Quantum Electron.* **37**, 414–417 (2001).
  30. L. Sulmoni, J.-M. Lamy, J. Dorsaz, A. Castiglia, J.-F. Carlin, W. G. Scheibenzuber, U. T. Schwarz, X. Zeng, D. L. Boiko, and N. Grandjean, "Static and dynamic properties of multi-section InGaN-based laser diodes," *J. Appl. Phys.* **112**, 103112 (2012).
  31. M. A. Cataluna, E. U. Rafailov, A. D. McRobbie, W. Sibbett, D. A. Livshits, and A. R. Kovsh, "Stable mode-locked operation up to 80°C from an InGaAs quantum-dot laser," *IEEE Photonics Technol. Lett.* **18**, 1500–1502 (2006).
  32. D. von der Linde, "Characterization of noise in continuously operating mode-locked lasers," *Appl. Phys. B* **39**, 201–217 (1986).
  33. F. Kéfélian, S. O'Donoghue, M. T. Todaro, J. G. McInerney, and G. Huyet, "RF linewidth in monolithic passively mode-locked semiconductor laser," *IEEE Photonics Technol. Lett.* **20**, 1405–1407 (2008).
  34. K. Merghem, R. Teissier, G. Aubin, A. M. Monakhov, A. Ramdane, and A. N. Baranov, "Passive mode locking of a GaSb-based quantum well diode laser emitting at 2.1  $\mu\text{m}$ ," *Appl. Phys. Lett.* **107**, 111109 (2015).
  35. X. Li, H. Wang, Z. Qiao, X. Guo, G. I. Ng, Y. Zhang, Z. Niu, C. Tong, and C. Liu, "Modal gain characteristics of a 2  $\mu\text{m}$  InGaSb/AlGaAsSb passively mode-locked quantum well laser," *Appl. Phys. Lett.* **111**, 251105 (2017).
  36. S. Becker, J. Scheuermann, R. Weih, K. Röbner, C. Kistner, J. Koeth, J. Hillbrand, B. Schwarz, and M. Kamp, "Picosecond pulses from a monolithic GaSb-based passive mode-locked laser," *Appl. Phys. Lett.* **116**, 022102 (2020).
  37. E. A. Avrutin and B. M. Russell, "Dynamics and spectra of monolithic mode-locked laser diodes under external optical feedback," *IEEE J. Quantum Electron.* **45**, 1456–1464 (2009).
  38. J. X. B. Sia, X. Li, Z. Qiao, X. Guo, J. Zhou, C. G. Littlejohns, C. Liu, G. T. Reed, W. Wang, and H. Wang, "1  $\times$  N (N = 2, 8) silicon selector switch for prospective technologies at the 2  $\mu\text{m}$  waveband," *IEEE Photonics Technol. Lett.* **32**, 1127–1130 (2020).
  39. B. Dong, X. C. de Labriolle, S. Liu, M. Dumont, H. Huang, J. Duan, J. C. Norman, J. E. Bowers, and F. Grillot, "1.3  $\mu\text{m}$  passively mode-locked quantum dot lasers epitaxially grown on silicon: gain properties and optical feedback stabilization," *J. Phys. Photonics* **2**, 045006 (2020).